Estimating S-N curves for local fiber dominated fatigue failure in ring specimens representing filament wound pressure vessels with damage

Eivind Hugaas*, Andreas T. Echtermeyer

Norwegian University of Science and Technology, NTNU, Trondheim, Norway

ABSTRACT

Modeling the effect of fatigue is important for predicting remaining life of damaged filament wound composite pressure vessels. This study shows how S-N curves can be measured that describe local fiber dominated fatigue failure on the scale of 0.25 mm near stress concentrations caused by a hole representing damage.

High frequency Digital Image Correlation DIC was applied to measure strain fields in rings tested by the split disk method. The rings were cut from a glass fiber reinforced polymer pressure vessel. A hole was cut into the rings to simulate damage in the laminate of the pressure vessel.

The Miner sum cumulative damage is calculated based on strain histories measured by DIC and several assumed S-N curves. The S-N curve giving Miner sum damage closest to the experimentally observed local failures in several samples is taken as the S-N curve describing the material´s behavior best. The local S-N curve was considerably less conservative than nominal S-N curves obtained from standard coupon testing. Its origin was a factor 2.5 higher.

1. Introduction

While local failure progression due to fatigue at large occurs in the matrix material, modeling local fiber dominated failure is important for knowing when and how catastrophic failure occurs [1–3]. This work is part of a larger program to better understand the long-term behavior of damaged composite pressure vessels and concentrates on filament wound composites. If composite pressure vessels are found to have damage in their load bearing laminate they are basically discarded and replaced by new ones. A better understanding of the remaining life with damage would help to make better decisions on the severity of damage. This study describes how S-N curves for local fiber dominated failure obtained from split ring specimens with a hole can be obtained and used to evaluate damage around strain concentrators in pressure vessels and as input for numerical analysis tools. The approach to obtain the S-N curves is unusual, deviating from common test procedures.

Typically S-N curves are measured from coupon samples cut out from flat plates tested in tension [4]. Samples are typically made from fabrics not representing the filament winding process well, but they tend have fairly homogenous characteristics throughout the specimen. One fatigue result is obtained per test with an ideally even (but cyclic) stress/strain level throughout the test volume. Strain gauges may be applied, but give only point-wise strains. Giancane et. al. [5] showed that strains in

a coupon test may vary extensively over the surface and may be much higher towards the grips than in the neck section, where strain gauges are typically placed [4,5]. This indicates that typical coupon testing gives conservative strain to failure curves. This is beneficial for design purposes, but hinders use of the materials full potential.

Fatigue testing samples with a stress raiser, such as a hole, change the situation. The strain field is not even anymore but shows a significant strain concentration. The strain field also changes with increasing number of fatigue cycles due to damage development (matrix cracking, splitting, undulation and delamination and progressive fiber failure) ([6]; Shen & Han, 2018). This occurs even in layers where the fibers are unidirectional and in the loading direction, as this paper shows. Fiber failure in the loadbearing layers will occur somewhere in small designated regions given by an unfavorable combination of high local strains and a statistically weak part of the material, as opposed to a coupon test, where failure may occur anywhere in the area between the grips just at a statistically weak spot [7]. In other words there will be a more direct correlation between the local strain and point of failure. The challenge with introducing a hole is the behavior of composites redistributing strain with increasing number of cycles. Since the fatigue strain at a point varies due to damage development it is not possible to relate the number of cycles of failure at that point to one fatigue strain and to build an S-N curve.

---

* Corresponding author.
E-mail address: eivind.hugaas@ntnu.no (E. Hugaas).

Fig. 1. Schematic of the DIC setup. Note that only the data from the camera monitoring the side that finally failed was used in this work.

This study presents a method that is capable of building an S-N curve from tests with a hole using high frequency DIC data. The high frequency DIC is capable of identifying local fiber failure and find local strain to cycle curves for the failing material points. Utilizing a back calculation method based on Miner sum calculations on the individual strain to cycle curves a best fit S-N curve is found. For a material with no statistical variation of properties each point of local fiber failure should show the same Miner sum value. The initially guessed S-N curve needs to be now changed until all failing points give a Miner sum value of 1. This fatigue curve describes local fiber failure. It is different from the S-N curve obtained by coupon tests that describes the catastrophic failure. In reality the scatter of material properties must be taken into account.

Other damage accumulation rules do exist, however, the Miner damage rule is the currently used rule in standards and industry [8]. Choosing the Miner sum approach is therefore a good starting point. But the presented method has good promise for comparisons of different damage rules. More sophisticated machine learning methods have been used to estimate and predict fatigue behavior, such as that by Wang [9], Rodriguez [10] and Mohanty [11] et al.. These methods do, however, use much less data than in this study and the results are fairly application specific. Combining machine learning and AI methods with DIC and other full field monitoring methods holds great promise for advanced fatigue lifetime modeling. This paper could provide data for that work.

Composite materials exhibit statistical variation in their properties like any material. Local variations related to the production process, such as void content, fiber density and fiber alignment also contribute to the scatter of properties. The number of cycles to failure for local fiber failure will, therefore, also vary. The ideal S-N curve mentioned above describing all local fiber failures does not exist. But it is possible to find an S-N curve that describes the local fiber failures on average and in a conservative way. The method presented here highlights how typical coupon test S-N curves are highly conservative for predicting local damage.

In this study it is not necessary to predict how the strain field changes during fatigue due to damage development as in a numerical model, because the strain field is measured directly by DIC. The aim is to obtain an S-N curve that can predict local fiber failure and subsequent catastrophic failure when enough local fiber failures have accumulated. The S-N curve for local fiber failure can be used in the future for modeling progressive failure under fatigue with finite element analysis. The S-N curve is found by a parameter study approach.

2. Materials and methods

2.1. Experimental setup

Four ring specimen with a hole cut from a filament wound pressure vessel were tested with a split disk setup. The hole was introduced to simulate damage. The split disk method was used as a simple and pragmatic alternative to costly pressure testing of the actual vessels. The ring specimen reflect well the material properties of the filament winding process. Flat coupon specimens, as typically used for fatigue testing, are difficult to produce with the filament winding process, since the fiber tension and alignment is hard to control [12]. Such specimens are often seen as not properly representing the properties of the filament wound component [12].

The tests were monitored with a system from Isi-Sys. Stingray F504B ASG cameras from Allied Vision Technologies (5 MP resolution) were placed on each side of the split disk setup. The cameras focused on the area around the hole, measuring 50*30 mm. Vic-2D, Digital Image Correlation (DIC) software, was used to analyze the images giving strain components. Fig. 1 shows the geometry of the setup and ring.

The split disks were manufactured from steel with a diameter of 140 mm and a width of 50 mm, the same as the ring specimen. The gap between the disks was 11 mm. Two cameras were employed, one on each side of the split disk setup as shown in Fig. 1. Both sides of the setup were monitored as it was not known which side would fail. Only the data from the camera on the failing side was used in the work presented in this article. Note, it is not known at the start of the experiment on which side of the ring failure will happen. The cameras were set to cover an area of roughly 50 mm by 30 mm on each side. As shown by M. A. Sutton et. al. [13] in plane 2D DIC strain errors are proportional to the out of plane motion relative to the distance from the camera to the specimen. Meaning that if the camera is placed far away from the specimen the error is less if there is any out of plane motion. For the ring specimen, the out of plane motion was small and the cameras placed far away (1.5 meter) relative to the potential out of plane motion. Also, the area in the camera frame was in good focus with only one camera. This allowed using a 2D system with sufficient measurement accuracy instead of a stereo system, simplifying the image processing. Using more than two cameras would have been beyond the capabilities of the image processing system. The cameras were timed to the load signal of the test machine taking pictures at peak load. The timing was checked using an external camera.
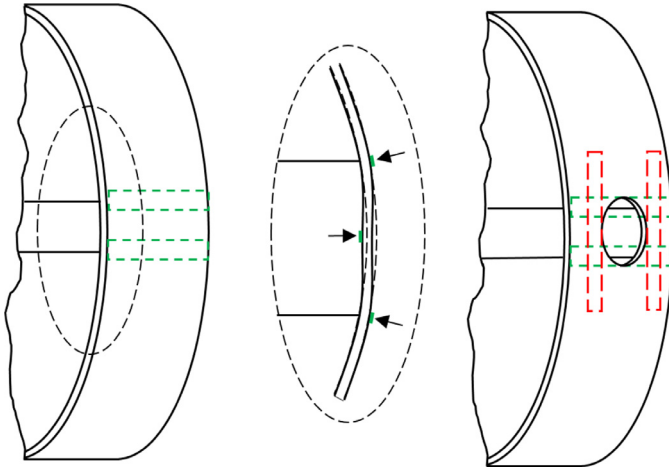
Fig. 2. Schematic of typical strain concentrations in a split disk test with a hole in the sample. Strain concentrations from bending are highlighted in green and the concentrations from the hole are highlighted in red. Arrows are used to further highlight the strain concentrations.

Table 1
Constituents and details on materials and production.

Constituent	Name/Type	Producer
Glass Fiber	HiPerTex W2020	3B [15]
Resin	Epikote MGS RIMR 135	Momentive [16]
Curing agent	Epikure RIMH 137	Momentive [16]
Curing time	15 hours at 80°C.	-
Mandrel	140 mm (outer) diameter polyethylene pipe	In house
Domes	Steel	In house

The split disk setup concentrates strain at the edges of the slit-disk on the outer surface and in the center inner surface due to bending [14], indicated in green in Fig. 2. The hole further concentrates the strain along the red squares. The setup therefor renders defined areas of expected failure.

2.2. Materials and pressure vessel fabrication

The pressure vessel was manufactured on a Mikrosan filament winding machine at NTNU. A polyethylene liner was used as a mandrel for winding. The layup was $[\pm89^\circ_2, \pm15^\circ_1, \pm89^\circ_2, \pm15^\circ_1]$ (Hoop/Axial/Hoop/Axial) from the outside to the inside of the ring ($\pm89^\circ_2$ fibers are on the outside), similar to a cross ply layup as found in most pressure vessels. Emphasis was put on having a hoop layer on the surface, enabling monitoring of a loadbearing layer with the DIC. No transition layers were used, the winding process was started anew for each layer. Also, the hoop layers had no woven pattern as for the axial layers. The hoop layers were as such wound with no filament running over the domes. The non woven nature of the hoop layers minimized any undulation of the fiber and made the fiber angle as close to the loading direction as possible. Fig. 3 shows the winding of the first axial layer of white glass fibers onto the black liner. Table 1 outlines the constituent materials. The ring cut outs were 50 mm wide. The liner was easily extracted from the cut outs as polyethylene does not bond to the epoxy. The holes were cut into the rings with a milling tool for composites (Seco Tools 40200-HEMI). They had a diameter of 20 mm. The geometry of the disks and the split disks can be seen in Fig. 1.

The strain to failure in fiber direction was measured previously in our laboratory for coupons made from the same fibers as used here. It varied between 22000 and 27000 microstrain for six test specimens, with the mean at 22150 microstrain. The fiber producer reports a strain to failure of 33000 mocrostrain [15]. The producer´s strain to failure is

considerably higher than the properties measured in our laboratory. The discrepancy is likely due to the manufacturer testing a more perfectly made material. Static and fatigue properties of the matrix were reported by A. Kraukalis et. al. in [17].

A microscopy study was carried out to assess variations in layer thickness and void content, properties that affect strain distributions. Looking at the microscopy image in Fig. 4 it can be seen that there is a considerable amount of voids in both winding directions and a considerable variation in layer thickness. The void content was not intentionally made high, despite the evidently high void content, standard procedures for filament winding production was followed. Similar imperfections have been observed in other filament wound structures [12]. Due to the high void content, no burn-off test was carried out to estimate fiber volume fraction as this would be artificially high with that much air/voids in the material. Also, the fiber volume fraction does not affect the results, which are strain based and not stress based.

2.3. DIC post processing

Digital Image Correlation, DIC, was used to measure the hoop strain (strain in the loading direction) on the surface of the outer layer. The test samples were painted with a speckle pattern and images (photos) taken with a 50 cycles period at maximum load. The cameras were triggered with the Fulcrum capture mode of Vic-2D using the load signal from the test machine as input. Vic-2D from Correlated Solutions was also used to analyze the images. A resolution sensitivity was run and a subset of 27 with a step size of 4 was found sufficient to capture the strain fields. The data was further exported from the software for post processing, where a resolution of 4 points per mm^2 was used which was found sufficient to match the original resolution of the step and subset size.

Some noise reduction was used on the data, employing a running average over 1000 cycles as shown on a representative strain vs cycle curve from a single data point in Fig. 5. Due to using a high resolution on the DIC images and variations in light over the testing time, some noise was present in the raw data.

2.4. Residual strain and Miner sum damage calculation

The DIC data contained strain at about 6000 points per frame (per measurement). In the following, frame is denoted i and strain as ε. Looking at only one point, the strain at frame 116 is then ε^{116}. It was assumed that the strain ε stayed near constant between two measurements. For each point and each measurement i the Miner sum was calculated using a strain based S-N curve, see Eq. 1.

$$M = \sum_{i=1}^{i} \frac{N(\varepsilon^i)}{N_{fail}(\varepsilon^i)} \tag{1}$$

$N(\varepsilon^i)$ is the number of cycles at strain ε^i; that is cycles between two measurements $i-1$ and i at the strain ε^i measured by the DIC. $N_{fail}(\varepsilon^i)$ is the number of cycles to failure for the strain ε^i. $N_{fail}(\varepsilon^i)$ is obtained from the S-N curve describing local fiber dominated fatigue failure. How this S-N curve is obtained is described in the results section. When the Miner sum reaches 1, theoretical failure happens.

All S-N curves are given by the general double logarithmic form in Eq. 2, alternatively formulated as Eq. 2.1.

$$\log\left(N_{fail}\right) = \frac{\log\left(\hat{\varepsilon}^O\right)}{\alpha} - \frac{\log\left(\varepsilon\right)}{\alpha} \tag{2}$$

$$N_{fail} = \left(\frac{\hat{\varepsilon}^O}{\varepsilon}\right)^{\frac{1}{\alpha}} \tag{2.1}$$

In case the S-N curve has a cutoff at the static strain, typical for glass fiber reinforced composites [3,7,18,19], Eq. 3 applies.

$$\log\left(N_{fail}\right) = \begin{cases} \frac{\log\left(\hat{\varepsilon}^O\right)}{\alpha} - \frac{\log\left(\varepsilon\right)}{\alpha} & for\ \varepsilon < \hat{\varepsilon} \\ \log\left(1\right) & for\ \varepsilon \geq \hat{\varepsilon} \end{cases} \tag{3}$$

Fig. 3. Winding of the first axial layer of the pressure vessel. Rings for testing were cut from the cylindrical part.
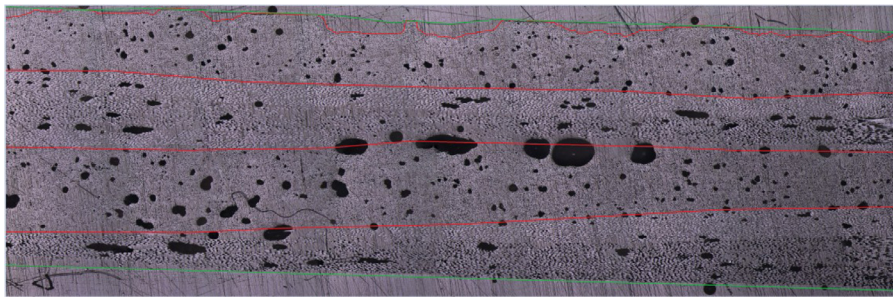

Fig. 4. Microscopy with layer borders shown in red and the bottom and top of the laminate shown in green. Many voids (black) are in the material. The outside of the vessel is in the top of picture. (Outside the green lines is potting resin holding the sample in place for polishing).
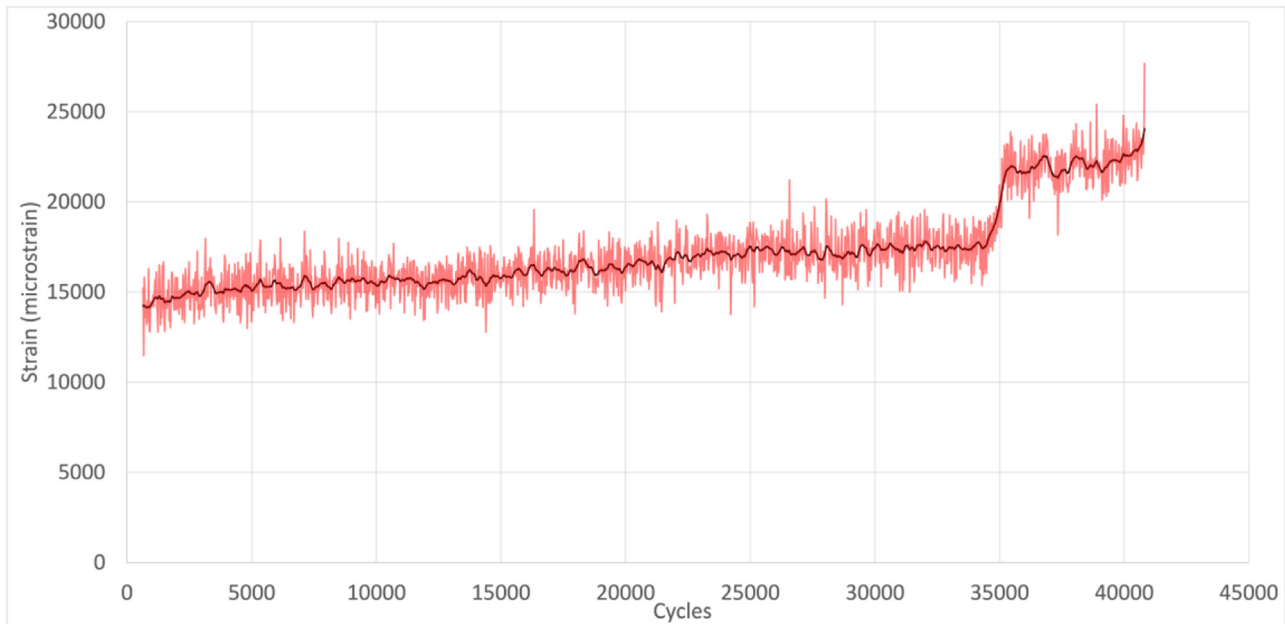

Fig. 5. Noise reduction example from a representative strain vs cycle curve of a single data point.

α describes the slope of the S-N curve, $\hat{\varepsilon}^O$ is the origin of the curve at cycle 1 and $\hat{\varepsilon}$ is the maximum static strain. If there is a cutoff, the failure cycle falls to 1 cycle as expressed by log (1) in Eq. 3.

Many studies have attempted to find composite material specific damage accumulation rules and S-N curves. Despite the effort, the same approach as for steel is still the preferred method in industry [8]. That is using the Miner damage accumulation rule and log log S-N curves. T.

P. Philippidis and V.A. Passipoularidis [20] made a review of residual strength models and compared them to experimental data. They made a short and concise conclusion that describes the state of the art well, cited here.

"The main conclusion is that the use of complicated phenomenological models requiring large experimental data sets for implementation does not necessarily pay back in terms of accurate predictions and con-
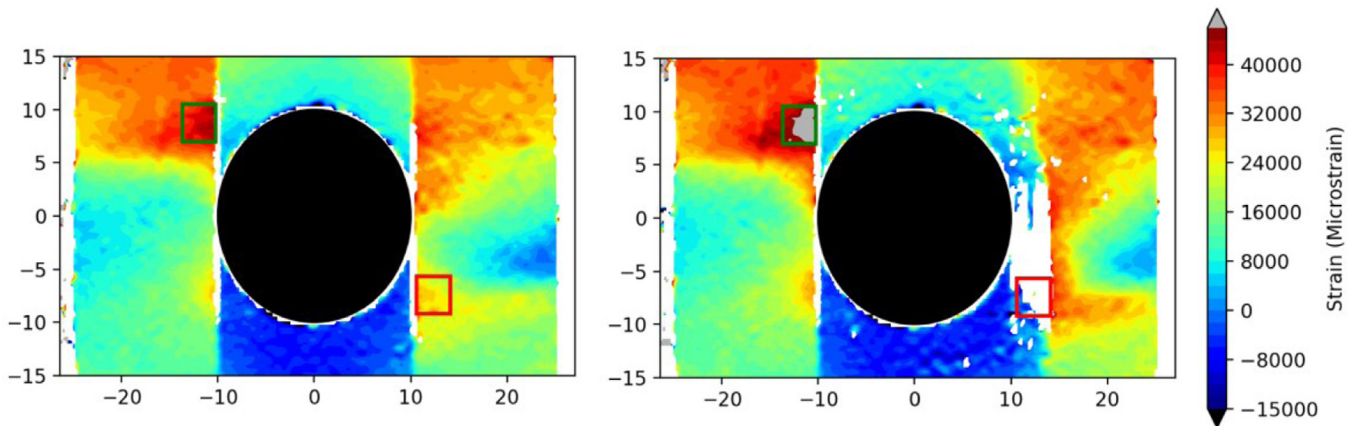
Fig. 6. Contour plots of hoop strains (vertical direction) of a static test measured by DIC in the ring specimen near the hole (black) at catastrophic failure (right) and just before (left). Failed material is shown as white. Failure initiated at the red square. The highest strain was observed in the green square.

sequently simple models requiring limited experimental effort should be preferred." Phillipidis [20].

The value of the Miner sum is often referred to as fatigue damage. However, this damage parameter has no direct physical meaning. It also does not reflect the remaining number of fatigue cycles to failure or remaining strength, because they will depend on the magnitude of the fatigue strain applied in the future. A Miner sum value of 1.0 is per definition the value for failure, however, the Miner sum may be bigger or smaller at failure depending on the scatter in fatigue properties inherent with the material. A more useful parameter is Hashin´s residual strength [21]. It calculates at which strain $\varepsilon_{residual}$ the material would fail if only one more cycle would be applied, expressed in Eq. 4.

$$\varepsilon_{residual}^i = \hat{\varepsilon}^O \left[1 - M^i\right]^\alpha = \hat{\varepsilon}^O \left[1 - \sum_{i=1}^{i} \frac{N\left(\varepsilon^i\right)}{N_{fail}\left(\varepsilon^i\right)}\right]^\alpha \quad (4)$$

Further an exposure factor f is defined in Eq. 5 as:

$$f^i = \frac{\varepsilon^i}{\varepsilon_{residual}^i} \quad (5)$$

If a strain ε^i is applied to a point in the sample, the exposure factor f^i describes how close the point is to failing. If f^i should exceed 1, local fiber failure would happen provided a perfect material without scatter.

3. Results

3.1. Static test results

A quasi static test was performed to obtain the static strain to failure. The contour plot of strain in the hoop direction when the ring failed and at the frame before is shown in Fig. 6. Initially the strain concentrations are at the two points described by the equator of the hole. Damage develops at these locations already at small loads as splits in the matrix along the fibers tangent to the hole. The splits are observable as white streaks tangential to the hole in the DIC contour plots in Fig. 6. Delamination and transverse matrix cracks also develop with increasing load and contribute to redistributing the initial strain field. Individual delaminations and transverse matrix cracking are, however, difficult to observe experimentally from the DIC data, as they develop inside the laminate and are only indirectly affecting the strain field. After splitting initiates, the peak strain concentration moves to the edges of the split disks from bending, indicated in green in Fig. 2. The shear splits may propagate further into the material, but due to the bending of the area between the disks, the strain concentrations do not follow the shear crack tip further. This is beneficial, keeping the peak strain within the DIC frame. It is contrary to coupon testing, where the shear split may travel with the peak strain

concentration all the way to the grips and give an invalid test. The details of the damage development are not scope of this paper, since the effect of the damage on the strain concentration is measured directly by the DIC.

A surprising result is that the highest strain of 40 000 microstrain is found near the upper left split, while failure initiated at about half that strain of 22150 microstrain at the lower right split in Fig. 2. These two areas of interest (AOI) are marked by a green and red square respectively. The load vs. strain curves for these two areas are plotted in Fig. 7, the two small circles indicate the two DIC frames in Fig. 6. The strain difference is big and is likely due to a varying distribution of imperfections, voids in particular as evident from the microscopy picture in Fig. 4. Variations in laminate thickness and delamination development are also important. Undulation of the fibers below the hoop layer may also contribute to strain changes. The strain to failure at the point where catastrophic failure initiated matches the strain to failure of 22000 to 27000 microstrain obtained from coupon tests in our laboratory The coupons were cut from flat plates made with the same constituent materials by filament winding. The measurements from conventional coupon specimen represent the lower bound of the material´s strain to failure obtained over a fairly large measurement volume (the gauge section of the coupon test). The scatter of the strength obtained from different coupon tests describes the variation of the lower bound of the material´s strain to failure. However, the strain at the other strain concentrations of the ring specimen tested here was nearly a factor two higher without causing any failure. This shows that the material can be locally much stronger than would be expected from a conventional test. Failure happens at the point where the material is locally weakened (due to voids etc.) Note: The DIC measures local strain with a resolution of about 0.5×0.5 mm². The strains on a microscale, e.g. around voids, may be higher, but are not detected.

3.2. S-N curve methodology

The aim of the test program was to find S-N curves that describe local fatigue failure of the fibers in the laminate. Three fatigue tests of rings with a hole were carried out. Strain fields at maximum load were measured frequently with DIC, as shown in Table 2.

While the static S specimen was analyzed in the above section, this section focuses on the fatigue specimens A – C. Contour plots of the maximum strain in hoop direction shortly before catastrophic failure are shown in Fig. 8. Regions where local fiber damage developed and accumulated are indicated by the black boxes. The black boxes are called here line slices and will be explained further down. White spots inside the line slices indicate local fiber failure. Similar to the static tests, the highest strain concentrations at failure are located at the edges of the
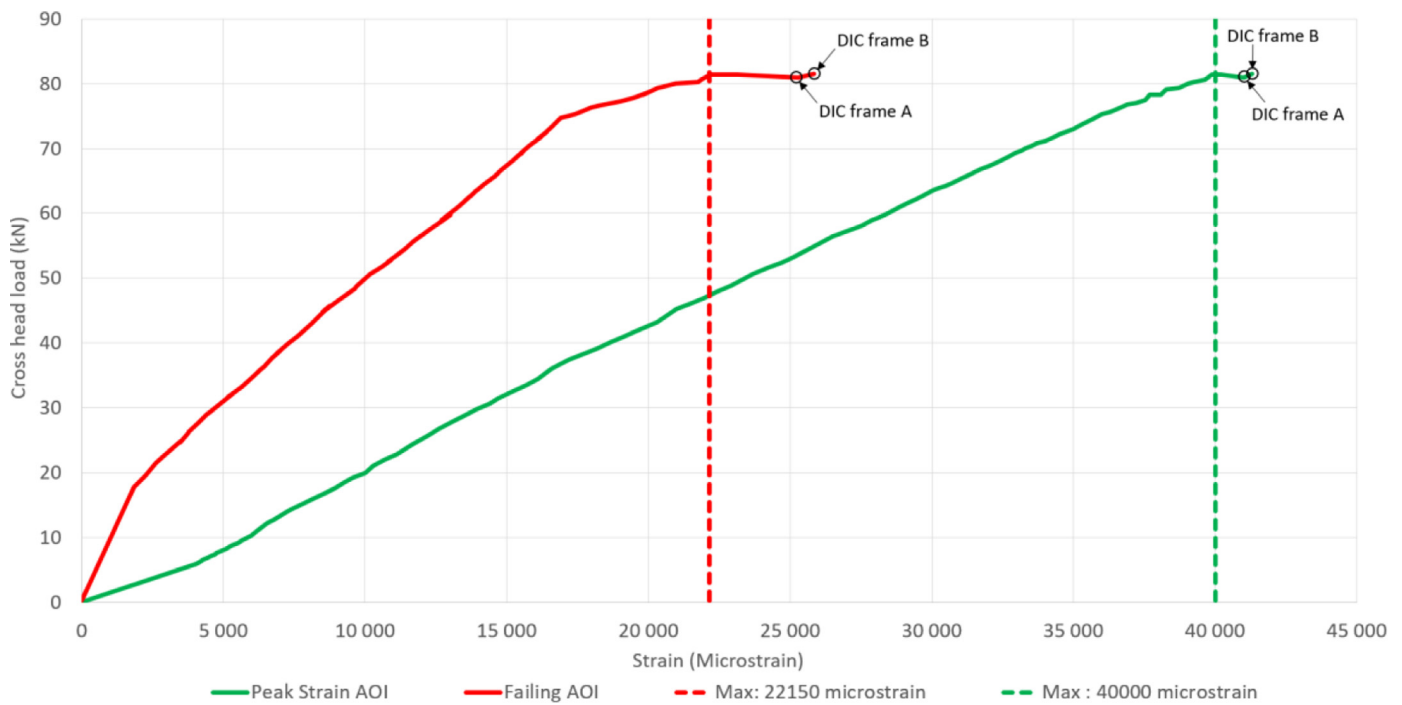
Fig. 7. Cross head load plotted against local strain curves of the ring specimen. The red and green curves represent where the specimen failed and where it had its highest strain, as indicated by the red and green squares in Fig. 6. DIC frame A and B indicate the left and right contour plot in Fig. 6.

Table 2
Failure cycle, loads and DIC frequency.

Sample	Load (kN)	Load ratio	Frequency	Failure cycle	DIC frequency
S	80.0	Started at 0.0 kN load	1 mm displacement/min	1 (Static)	1 per sec after 10 kN
A	45.0	0.1 (min load = 4.5 kN)	1 Hz	40820	1 image per 25 cycles
B	43.0	0.1 (min load = 4.3 kN)	1 Hz	65360	1 image per 25 cycles
C	40.0	0.1 (min load = 4.0 kN)	1 Hz	127768	1 image per 50 cycles
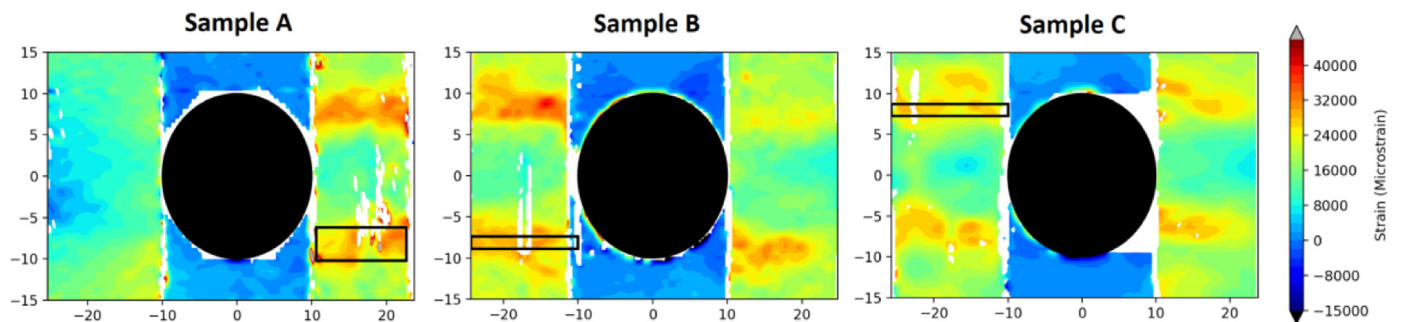
Fig. 8. Contour plot of hoop strains (vertical direction) measured by DIC in the ring specimen near the hole (black) close to fatigue failure. Failed material is shown as white. Catastrophic fiber failure initiated in the line slices (black boxes) after accumulation of local fiber failure in the line slices. Failure is shown for three specimens A, B and C failing after 40820, 65360 and 127768 cycles respectively.

split disks. There are also prominent shear cracks extending along the tangent to the hole for all specimens. Contrary to the static test however, the strain is more spread out, and the strain concentrating effect of the hole is non-existent upon failure. Fig. 9 shows the strain across the line slice in Specimen C for different numbers of cycles and shows how the strain concentration lessens and moves over time. Fig. 10 shows the contour plots at the corresponding cycles. At 364 cycles the highest strain is located close to the split that grew vertically (in load direction) out of the hole. This strain concentration moves progressively towards the edge of the specimen while also gradually lowering relative to the average strain over the line slice. Finally it ends up close to the edge of the specimen where a separate strain concentration develops and final

failure occurs. This shows that local damage developing under fatigue (matrix cracking, delamination, fiber-matrix debonding) is beneficial for reducing the strain concentrations and can cause fiber failure away from the expected point of failure. As seen in the contour plots however, the strain concentration along the equator of the hole stays close to the hole throughout the cycling. Here the mean strain is too low for matrix cracking to occur and the strain field stays relatively stable. It further highlights how matrix damage changes the load distribution between the fibers.

The aim of this paper is to find S-N curves that describe local fiber failure on the scale of about 0.25 * 0.25 mm, as typically used in modeling. Local fiber failure happens very shortly before catastrophic failure.
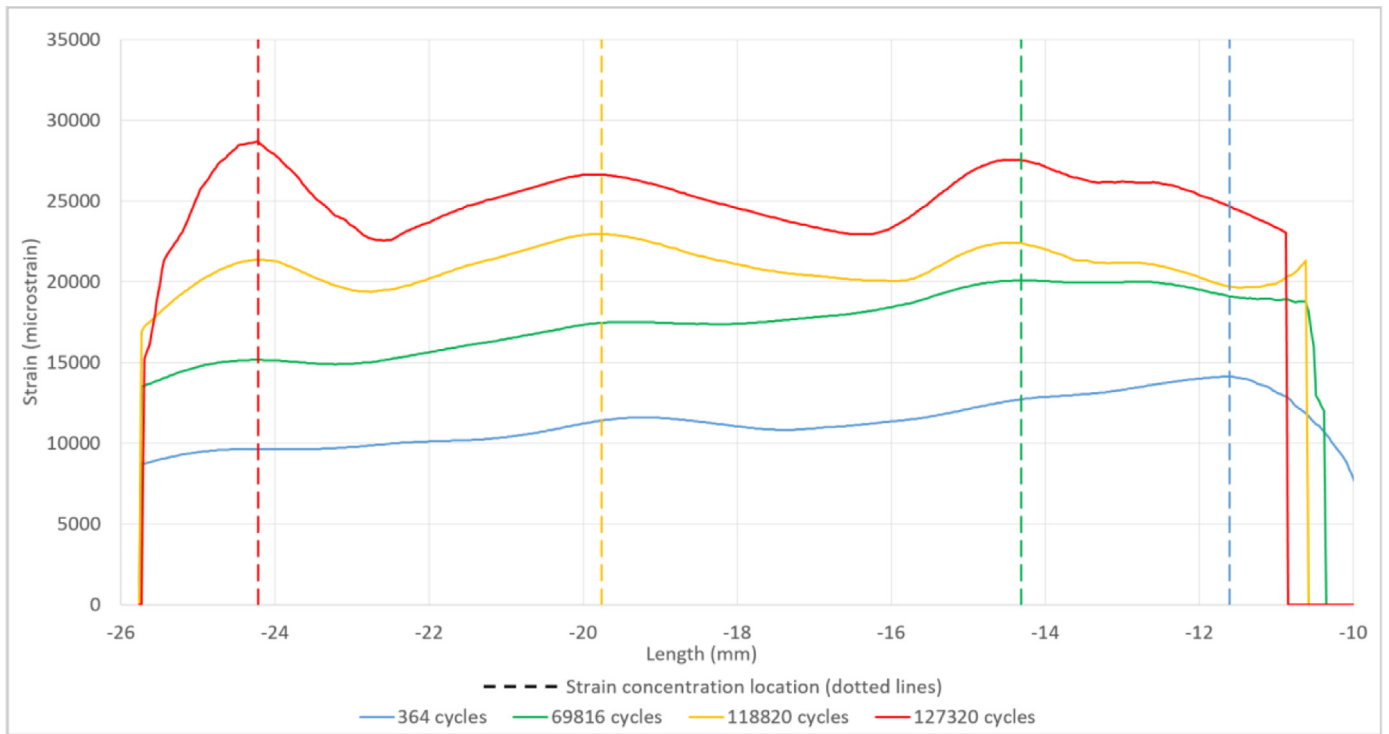
Fig. 9. Strain across the line slice on the upper left in specimen C (see Fig. 8). The edge of the hole is located at -10 on the x-axis. The highest strain moves from the edge of the hole towards the outer edge of the specimen.
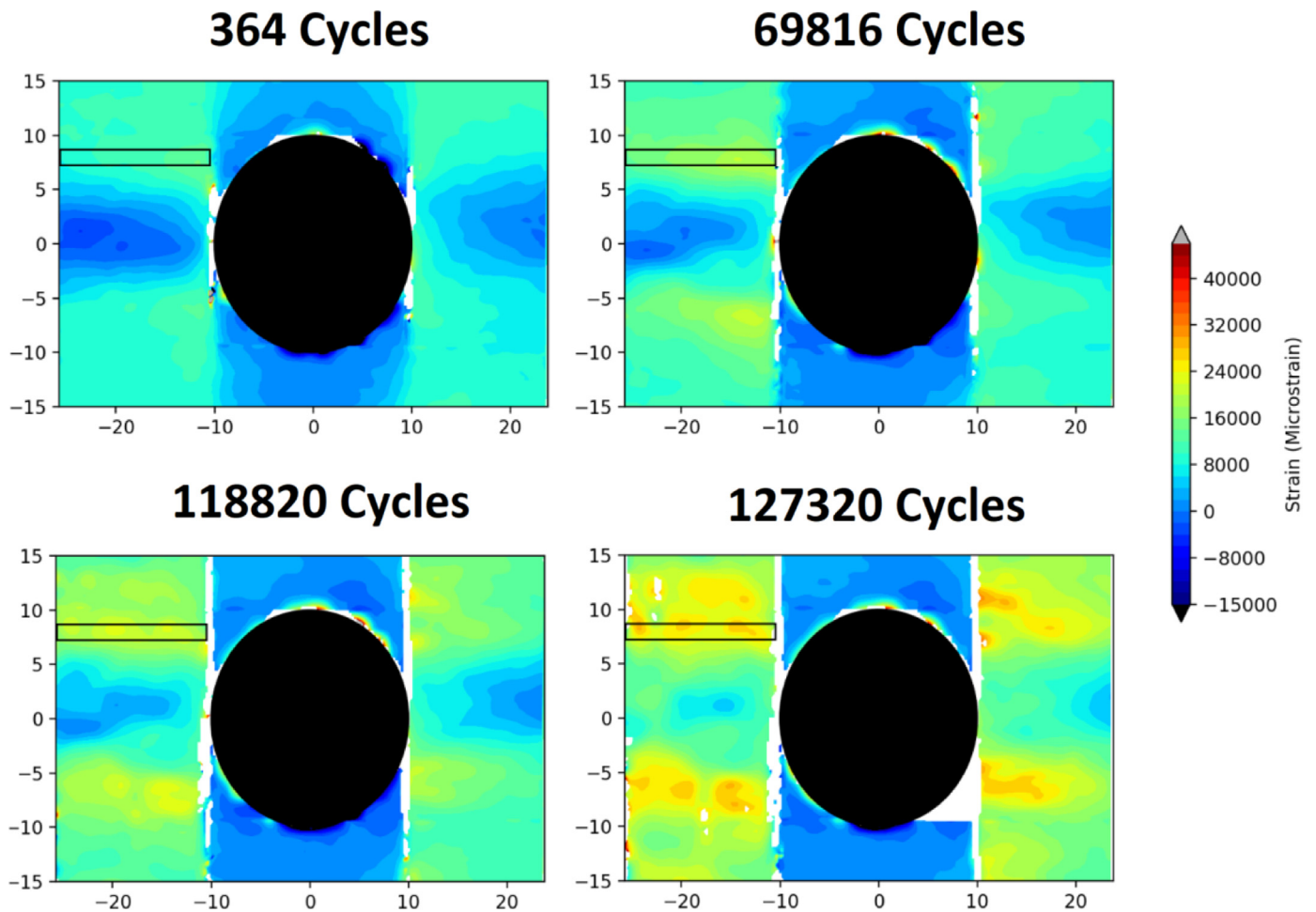
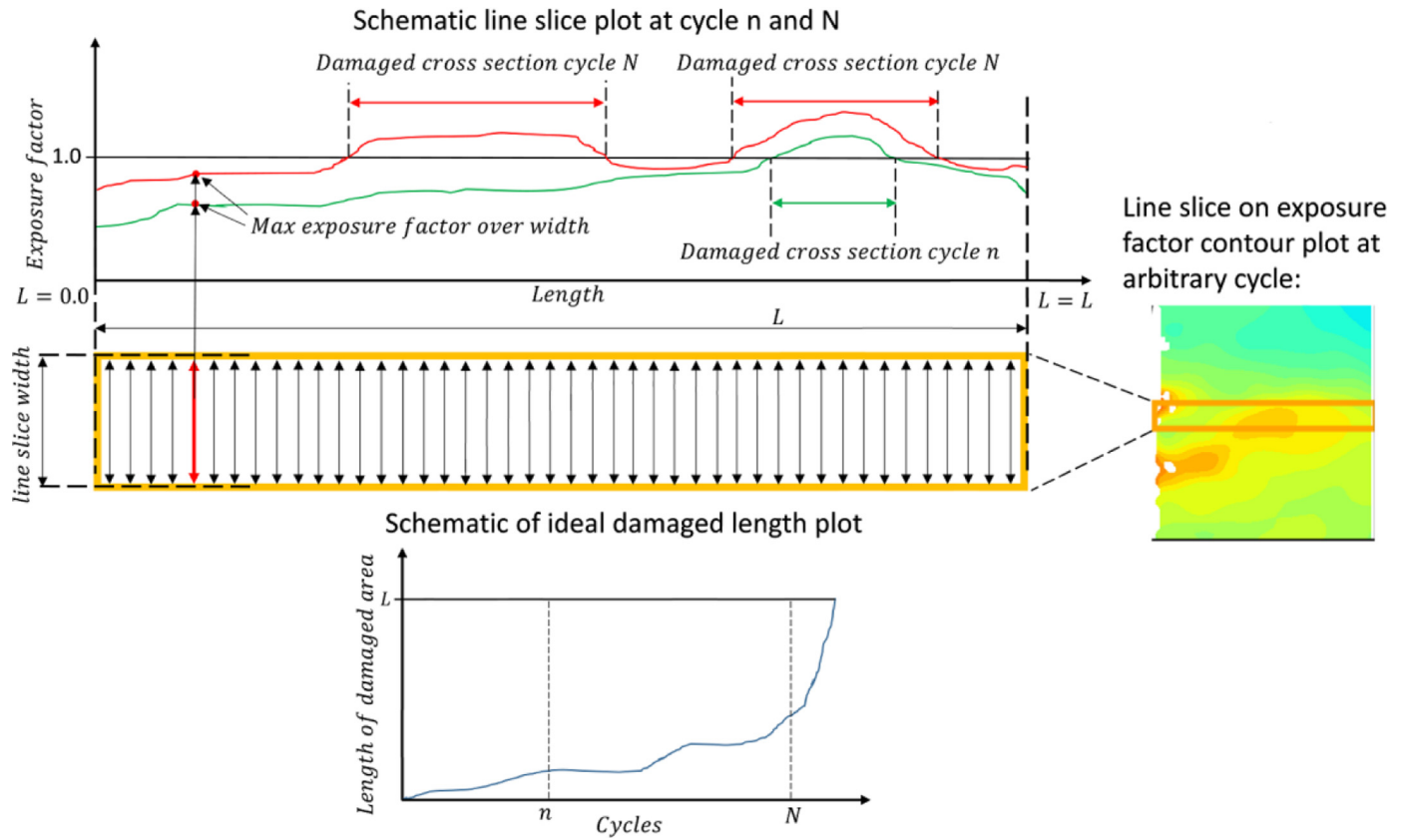**Fig. 10.** Contour plots for the four strain curves in Fig. 9.

Fig. 11. Schematic showing how damaged cross section was defined over the line slice length and how an ideal S-N curve should predict damage.
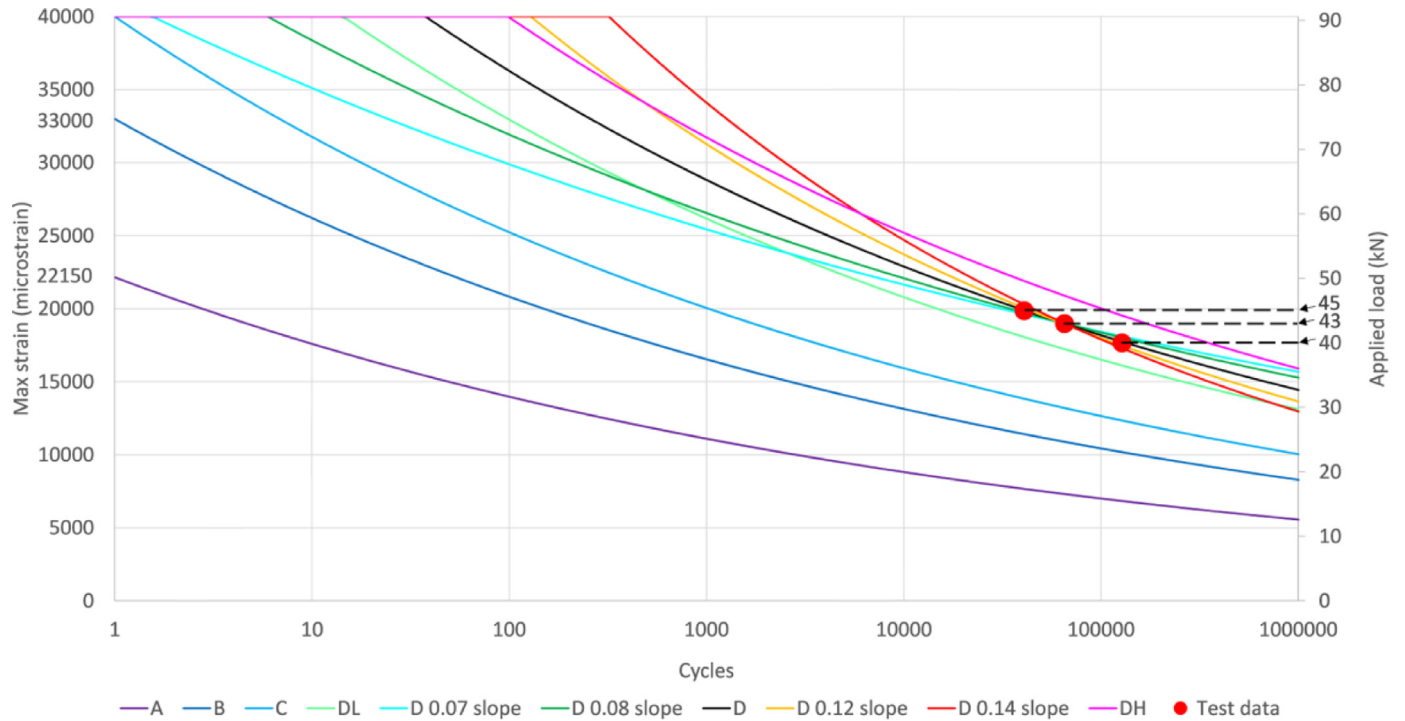

Fig. 12. Comparison of predicted catastrophic fatigue failure based on S-N curves from Table 3 and experimental results.
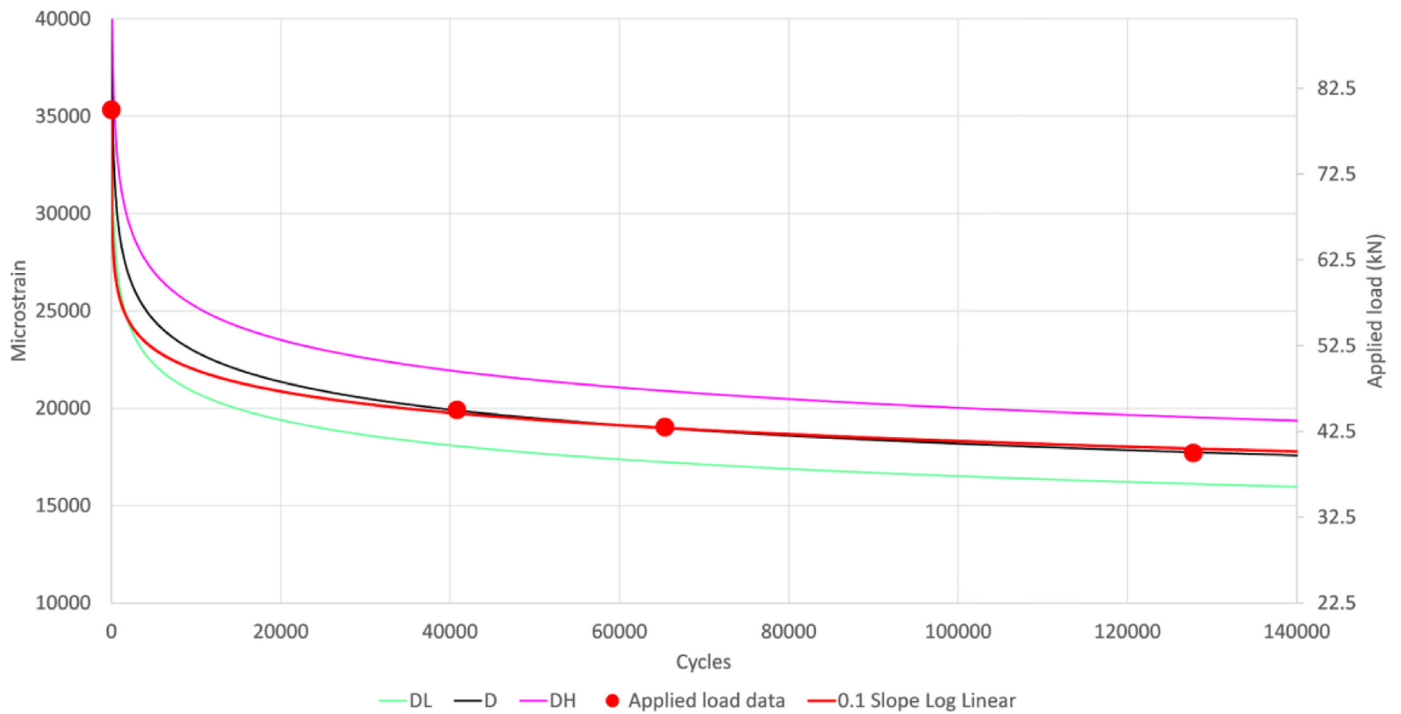
Fig. 13. Log Log plotted against Log Linear curve showing little difference at the same slope of 0.1.
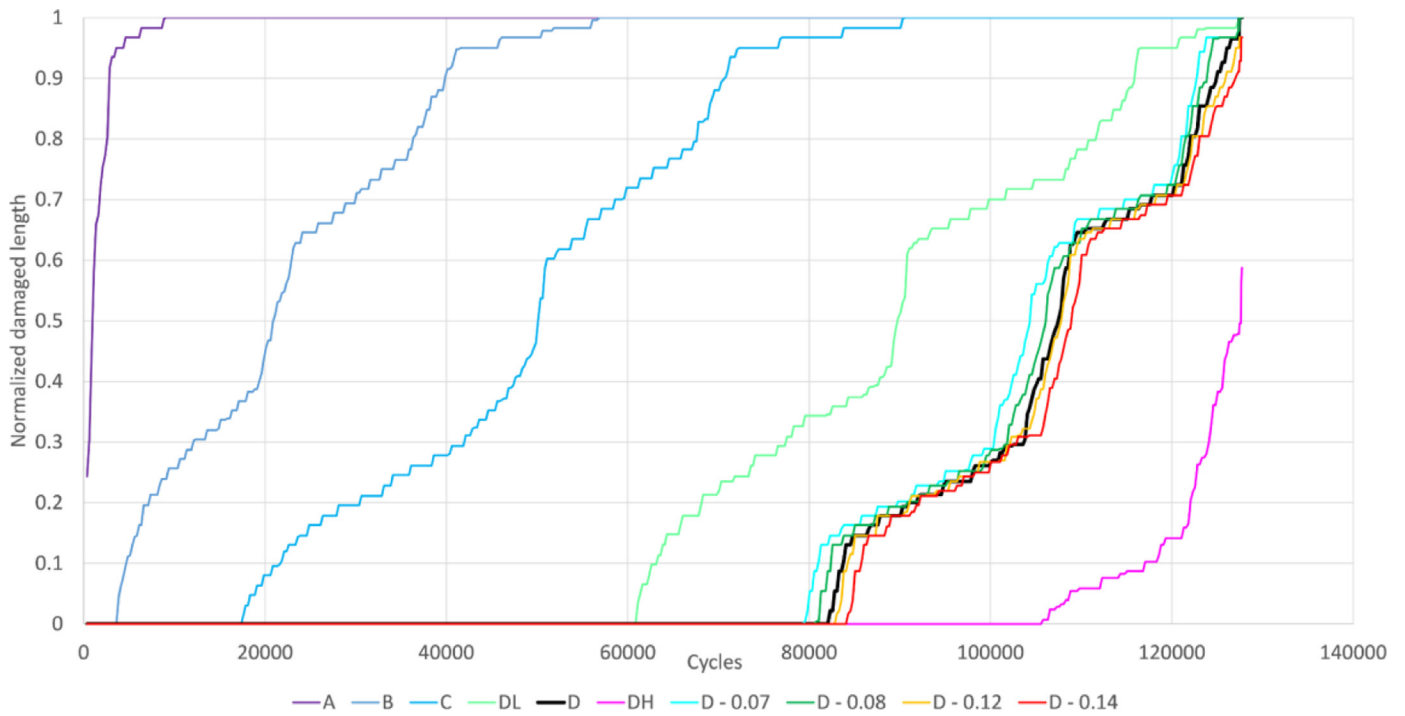
Fig. 14. Normalized damaged length for specimen C for the SN curves given in Table 3.

By measuring strains directly by DIC over the entire lifetime of the specimen the proper strains experienced by the fibers at every point (within the resolution of the DIC system) throughout the specimen are measured directly. The reasons for the changes of the strain do not need to be known, which is an advantage of using DIC.

S-N curves are normally found by regression of stress or strain vs. cycles to failure data from coupon testing. The standard coupon sample has an even strain field and will fail at the weakest point, as described for the static results. This approach is sound for conservative design estimates in the industry, but it falls short of giving the full picture of the material´s behavior in the presence of strain concentrations as needed in numerical models for describing damage development. Understanding the behavior of components with strain concentrations requires knowledge of the local properties throughout the specimen, not just the weakest spot in a larger volume obtained from coupon tests.

Fatigue testing a specimen with a hole and using DIC measurements allows measuring the local strains vs. number of cycles at many points of the test specimen. If the strain field would not change, local S-N curves
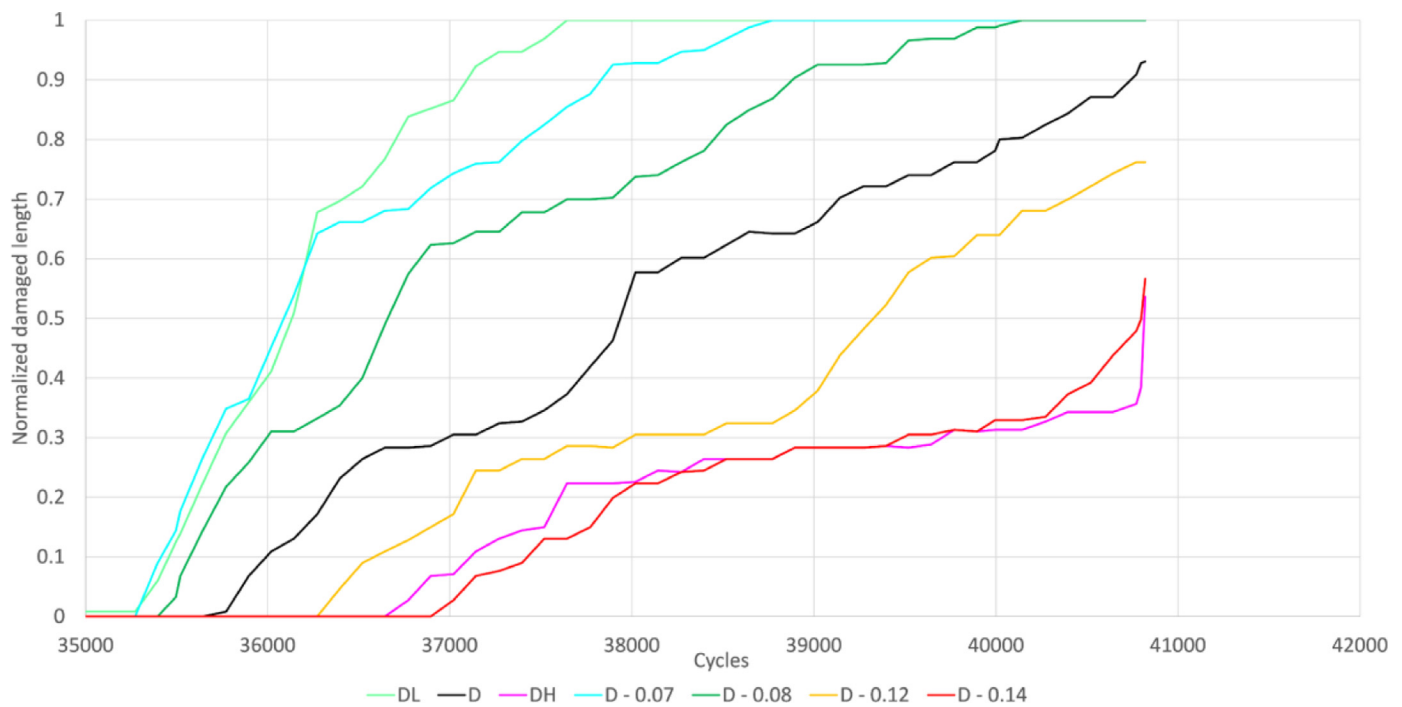
Fig. 15. Normalized damaged length for sample A for the SN curves given in Table 3.

could be obtained by just measuring local strains vs. number of cycles to local failure. However, as shown in Fig. 9 and Fig. 10, local strains change with increasing number of cycles, prohibiting the direct measurement of S-N curves at local points. This necessitates an approach for obtaining S-N curves that can take into account varying strains over time.

In this study the varying strains are handled by calculating the Miner sum from the local cyclic strains measured by DIC and an assumed S-N curve. The Miner sum is calculated and updated after every DIC measurement interval. It is assumed that the strain is constant within a measurement interval, which should be a reasonable assumption considering the large number of measurements. This approach is equivalent to how fatigue damage may be handled in existing models, numerical and analytical. However, numerical models have to adopt a cycle jump approach that assumes and estimates damage over a large range of cycles [22]; simulating each cycle is too numerically expensive. By instead calculating the Miner damage on the actual strains in the specimen from high frequency DIC, a more accurate evaluation of the S-N curve and damage rule emerges with a lot less assumptions than in an equivalent numerical model.

Since first local fiber failure and catastrophic failure happened within a short cycle span, around 500 cycles for all tests, the proper S-N curve should also predict catastrophic failure. Catastrophic failure is here assumed to happen when the whole length of the line slices have a Miner sum/exposure factor over 1.0. Looking at where the line slices are located, this means that the whole cross section on one side of the hole has theoretically failed. This choice is further supported by the even strain fields in Fig. 9 and the fact that fiber failure occurred away from the hole.

To evaluate the choice of different S-N curves for properly describing fatigue damage and catastrophic failure with the Miner sum approach, the length of local theoretical fiber damage along a line slice was determined, as explained in Fig. 11. For each point along the length of the line slice at each cycle, the algorithm searches over the width of the line slice for an exposure factor above 1.0. If it finds this, the length point along the line slice is set as damaged. For the ideal S-N curve, the damaged length should be equal to the line slice length upon catastrophic

Table 3
S-N curve parameters.

Name	Parameters		
	Origin (microstrain)	Slope	Cut-off (microstrain)
A	22150	0.1	22150
B	33000	0.1	33000
C	40000	0.1	40000
DL	52222	0.1	40000
D	57500	0.1	40000
D – 0.07	41254	0.07	40000
D – 0.08	46141	0.08	40000
D – 0.12	71643	0.12	40000
D – 0.14	89719	0.14	40000
DH	63312	0.1	40000

failure. Any curve that predicts a damaged length over the whole line slice before failure is conservative.

The presented method assumes that once a local point has a miner sum/exposure factor over 1.0, local fiber failure may happen at this point. When a whole cross section has a Miner sum/exposure factor over 1.0 fiber failure may progress over the cross section and initiate catastrophic failure.

3.3. Evaluating different S-N curves

In order to find a suitable S-N curve that can predict failure of the test specimen, the S-N curves listed in Table 3 were investigated. Note, cyclic fatigue strains are given as maximum strains, not amplitude strain. A traditional S-N curve has two variables; origin and slope. In case the origin is higher than the static strain to failure, a cutoff at the failure strain is necessary, as described in Eq. 3. Cutoffs are common for glass fiber composite material systems [7]. The S-N curves are also shown in Fig. 12.

The S-N curve "A" represents a typical S-N curve obtained from coupon testing. The static strain to failure of 22150 microstrain from coupon lab testing is used as the origin and the slope of the curve is 0.1, as typically found for glass fiber laminates [3,18,23–28]. The slope of
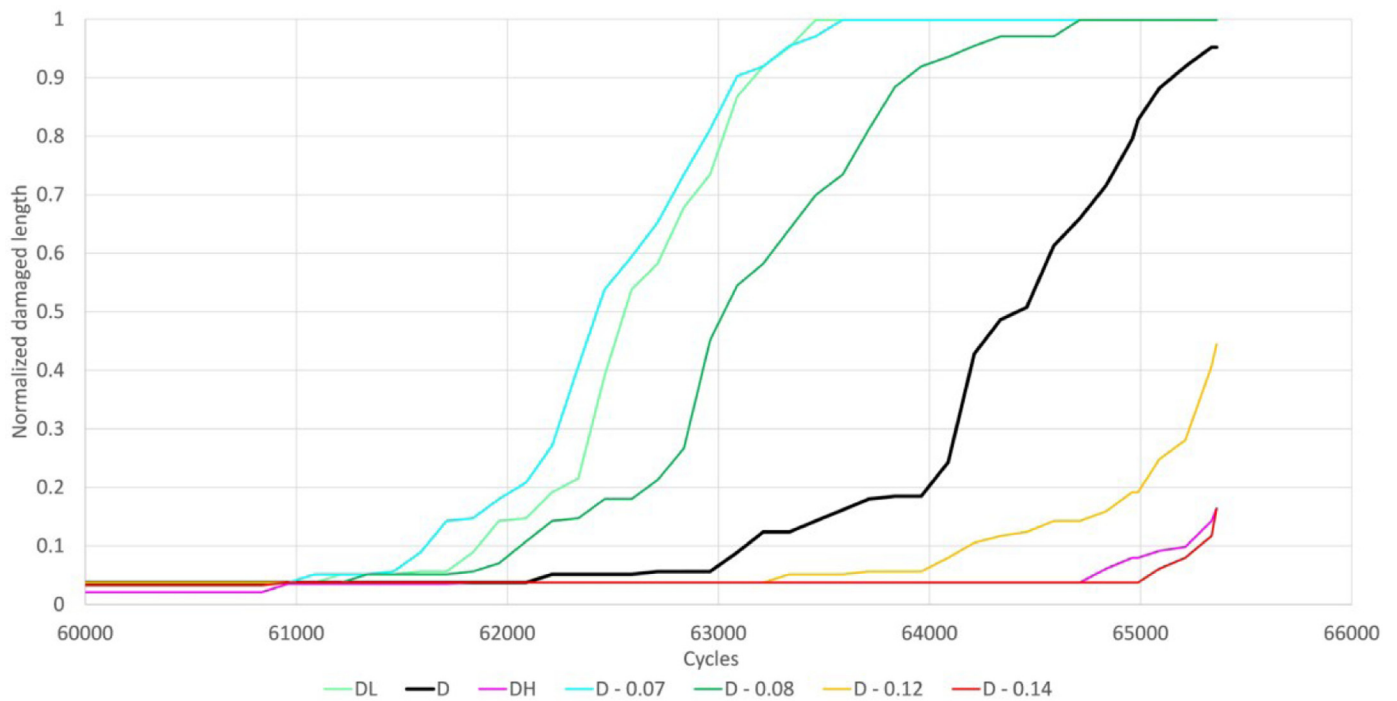
Fig. 16. Normalized damaged length for sample B for the SN curves given in Table 3.

Table 4
Summary of the different S-N curves damage prediction at the failure cycle.

S-N Curve	Specimen A		Specimen B		Specimen C	
	Damaged length	At cycle fraction	Damaged length	At cycle fraction	Damaged length	At cycle fraction
A	1.00	0.02	1.00	0.56	1.00	0.07
B	1.00	0.21	1.00	0.93	1.00	0.44
C	1.00	0.60	1.00	0.94	1.00	0.71
DL	1.00	0.92	1.00	0.97	1.00	0.99
D	0.93	-	0.95	-	1.00	0.99
D –0.07	1.00	0.95	1.00	0.97	1.00	0.99
D – 0.08	1.00	0.98	1.00	0.99	1.00	0.99
D – 0.12	0.76	-	0.44	-	0.97	-
D – 0.14	0.57	-	0.16	-	0.97	-
DH	0.54	-	0.16	-	0.59	-

the S-N curve for local failure should arguably be the same as for failure in larger volumes from a coupon test. This approach has also been applied by other studies investigating local properties (Eliopoulos & P. Philippidis, 2011). This investigation tested only three fatigue samples, which is not enough to establish the slope of the global S-N curve reliably, but it is sufficient to show the concept of obtaining S-N curves for local fiber failure. However, for the three tests, the typically used slope of 0.1 was found as the best regression fit based on the load vs. cycle data, as plotted on the second axis in Fig. 12. Most studies ([3,18,23–27]; Eliopoulos & P. Philippidis, 2011; [29]) use a log linear formulation for the S-N curves with a slope of 0.1, but the difference compared to a log-log S-N curve is small as shown in Fig. 13. A log linear formulation could have been used, but the best experimental fit was found with the log-log presentation in this study.

Fig. 14 shows the damaged length vs. number of cycles in the line slice for specimen C. The S-N curve "A" predicts that the entire length has failed after about 1000 cycles, while the real catastrophic failure happened at 127768 cycles. The traditional S-N curve as typically measured from coupon tests would predict a far too short lifetime. Predictions of the lifetime for samples A and B were also much too short. Fig. 15 and Fig. 16 shows the damaged length for samples A and B and Table 4 summarize the results.

The same analysis was done for the other S-N curves. These curves were shifted up relative to the "A" curve with the origin at 33000, 40000 and 52222, 57500 and 63312 microstrain respectively. All curves with an intercept higher than 40000 microstrain have the designation "D". DL and DH represents a low and high S-N curve while "D" curves with a designated number have a slope variation. The slope variation curve were scaled according to best fit around the applied load data assuming the D curve and the applied load data coalesced. This can be seen in Fig. 12 as the D curve and the best fit to the applied load data coalesce at all cycles after the cutoff cycle of the applied load curve. The cutoff is different for the applied load curve and the D curve and therefor the axis for the applied load data is shifted to above the maximum static load. Note, a cutoff was applied as given in Eq. 3, because the static strain to failure for the strongest part of the material cannot be exceeded.

It can be seen from Table 5 and Fig. 14 - Fig. 16 that S-N curves "B", "C" and "DL" gave too extensive damage predictions for all specimen. Curve "D" (with a slope of 0.1) gave damage predictions very close to the entire cross section and DH gave a damaged length short of the cross section. The "At cycle fraction" column tells at what fraction of the catastrophic failure cycle in Table 2 the S-N curve predicted failure across the whole line slice.
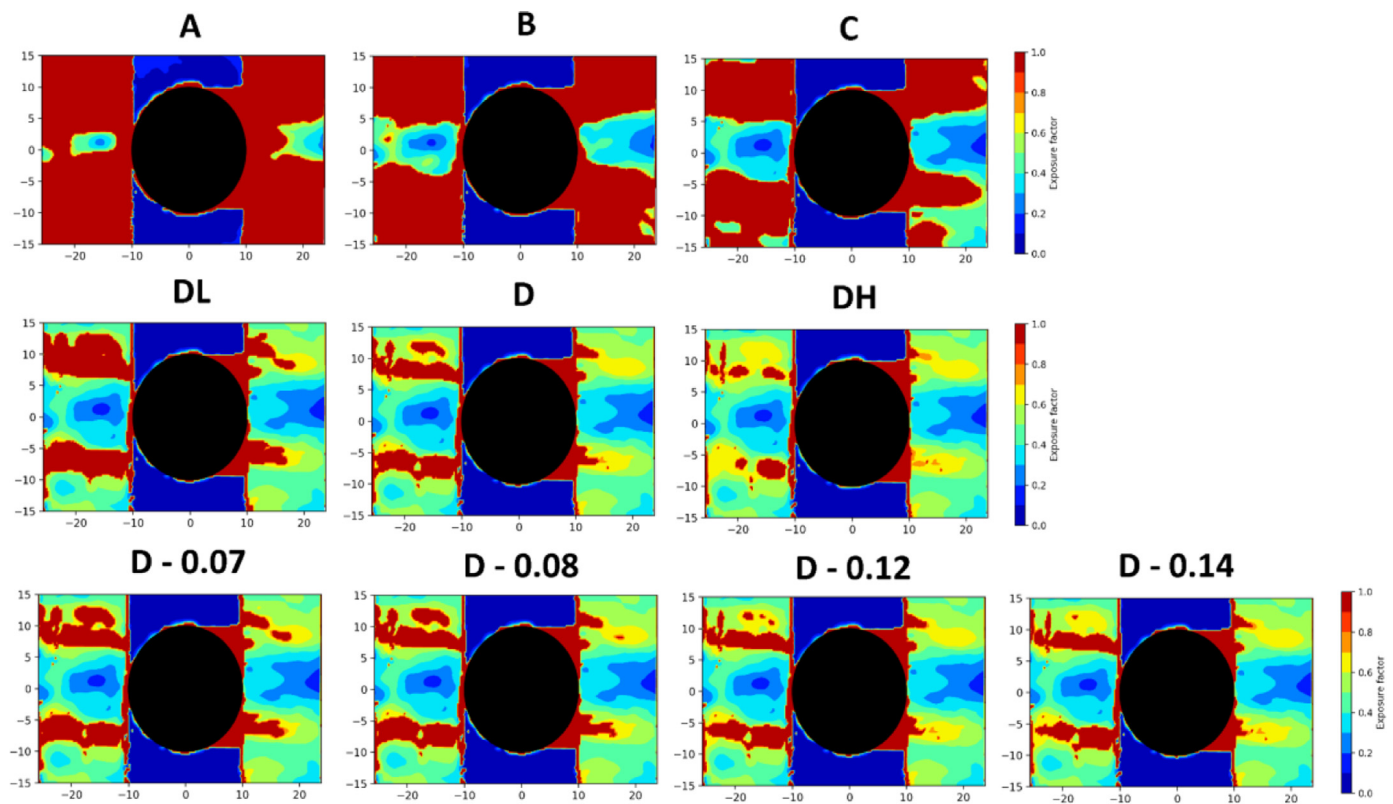
Fig. 17. Contour plots of exposure factor at catastrophic failure over sample C for all tested S-N curves.
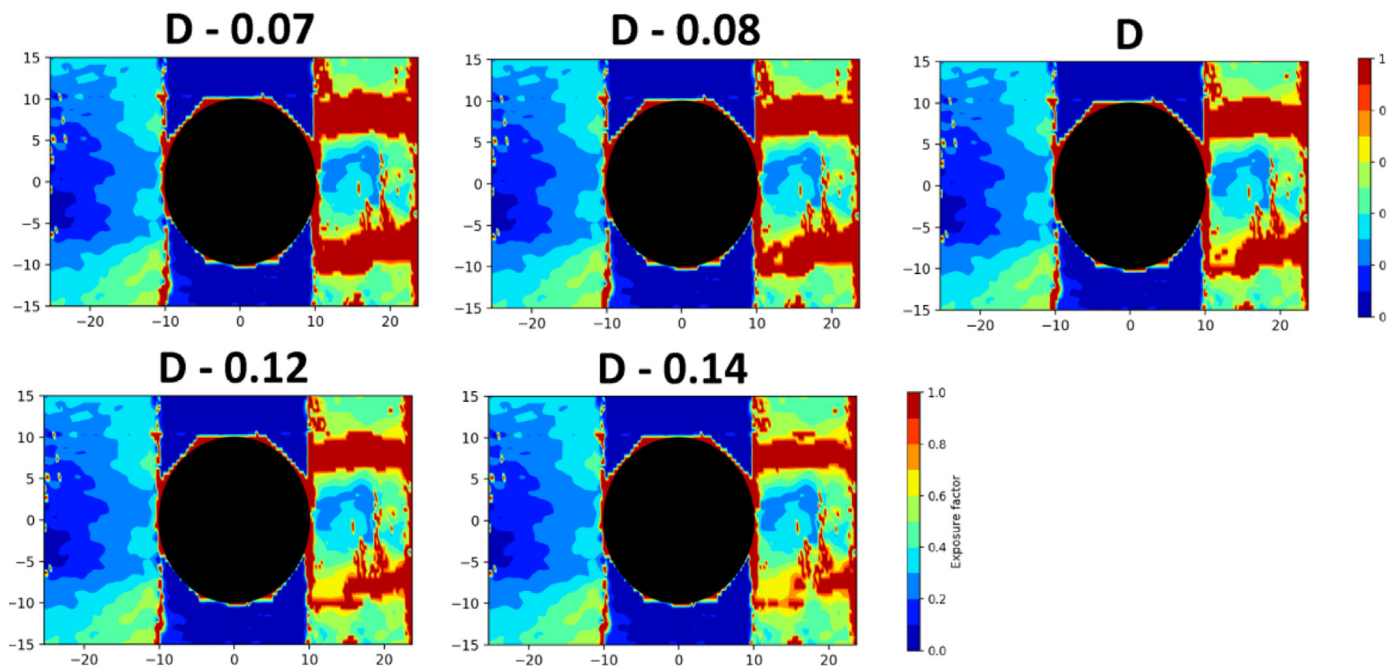

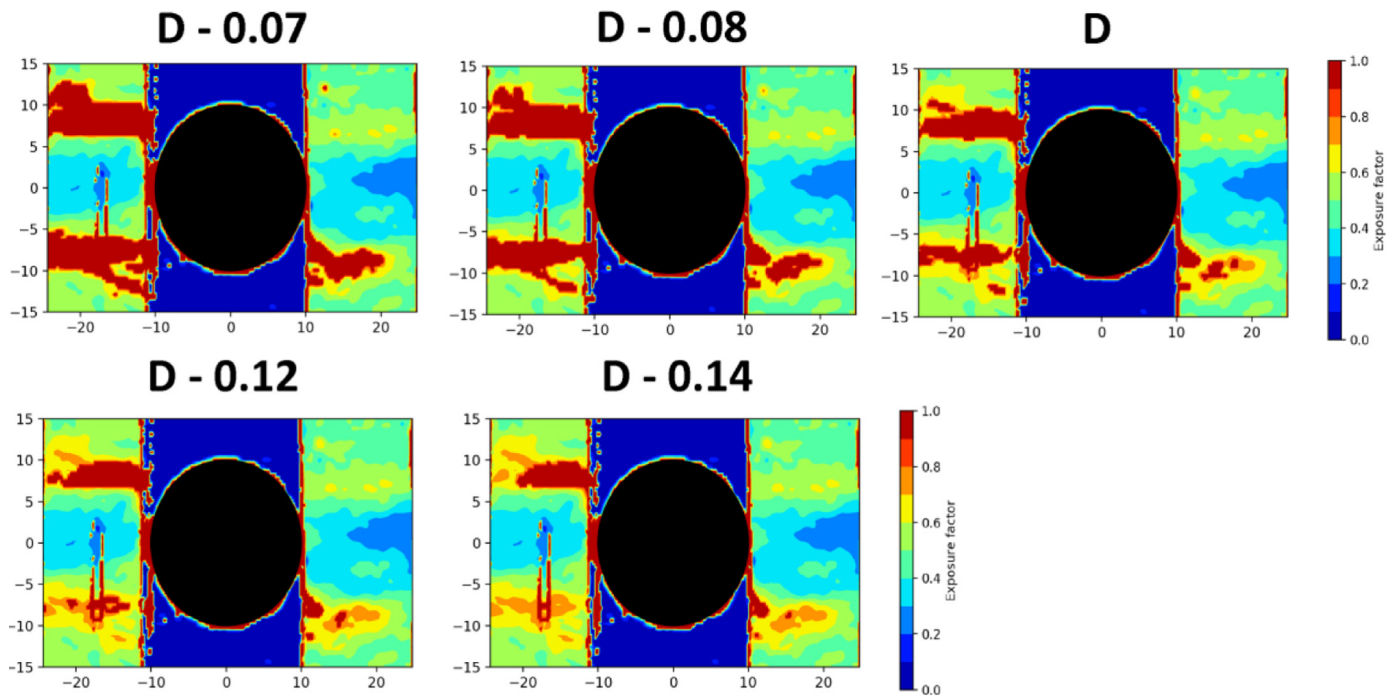**Fig. 18.** Contour plots of exposure factor at catastrophic failure for slope sensitivity S-N curves for sample A.

To check the sensitivity of the results to the slope, the slope of the "D" curve was changed from 0.07 to 0.14 as shown in Table 4. It can be seen that the C specimen´s damage is not affected by the slope sensitivity, while A and B is to a great extent. This is due to that A and B have higher strains and a shorter cycle span where fatigue damage occurs. Looking at the S-N curves in Fig. 12 it can be seen that it is particularly for the low cycle regime where the slope variation shows the biggest

differences. It is however remarkable that the D-curve's slope of 0.1 gives the most consistent damage prediction, in line with the slope found from literature and from the global load test data.

The difference in damage development between specimen A, B and C is due to a less sudden failure of the bottom hoop layer for Specimen C, giving a slower transfer of force from the bottom to the top hoop layer compared to A and B. It is evidently not possible to monitor the bottom

Fig. 19. Contour plots of exposure factor at catastrophic failure for slope sensitivity S-N curves for sample B.
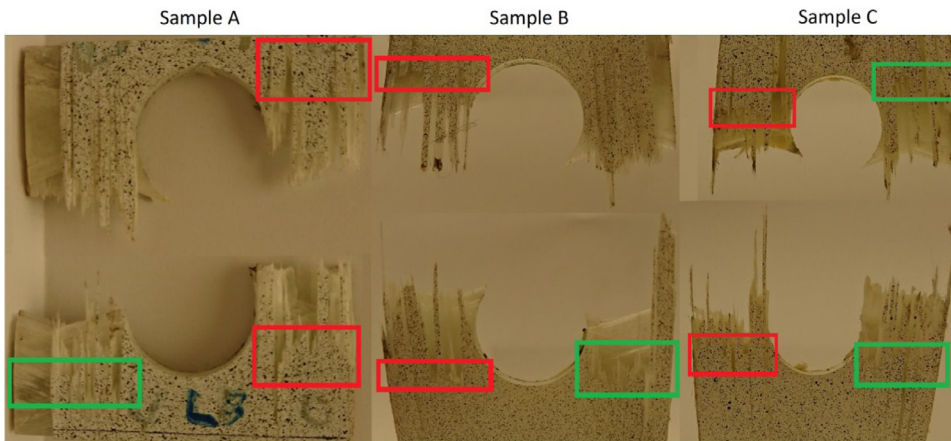

Fig. 20. Photos of the catastrophic fracture of the three samples. The main initial fracture surfaces are outlined in red squares. Further damage resulted from pulling the specimen apart and are highlighted in green.

hoop layer by any practical means, but it was observed visually that this layer failed more gradually for Specimen C.

Applying the exposure factor from Eq. 5.0 it can be shown how close the fibers are to failure theoretically. The exposure factor will change depending on the S-N curve used for calculating the Miner sum. Fig. 17, Fig. 18 and Fig. 19 show the contour plots of exposure factors for samples C, A and B respectively just before catastrophic failure. Exposure factors for specimen C are given for all S-N curves. Specimens A and B show only exposure factors for the slope sensitivity S-N curves.

Comparing the results with Fig. 19, where the experimental catastrophic failure is shown allows evaluation whether the predicted accumulated local fiber damage from the chosen S-N curves corresponds to the experimental failure.

Using the S-N curves "A", "B" and "C" in the exposure factor calculations overestimates damage; almost the whole sample is red, also reflected in the failed length graph in Fig. 14 - Fig. 16. This is further confirmation that these S-N curves are not suitable to predict local fiber failure. The damage calculated for the D curves are all reasonable. All show local fracture across the width on one side of the hole and most damage where the sample actually failed. Evident by looking at the time

history expressed in the failed length graphs, the D curve (with a slope of 0.1) gives the most consistent damage prediction across specimens. Variations of the slope around 0.1 can be seen to give less consistent damaged length prediction. The ability of predicting the progression of fiber failure is as important as identifying initial location of damage. The D curve can be seen to predict red areas in the contour plots also where the green squares are located in Fig. 20 for the C and B samples. For the A sample, the exposure factor is highest on the side of the hole where the damage progressed (bottom left).

Since the "A" curve is representative for an S-N curve obtained from coupon data for the material, it can be seen that such a curve would largely overestimate the local fiber damage development in the sample. When attempting to model fatigue damage growth numerically, using the right local fatigue properties will be critical for the success of such models. The method described here allow obtaining such local S-N curves for fiber failure in a still conservative way and highlights how standard coupon test S-N curves may be insufficient for describing local damage development.

Knowing the local S-N curves for fiber failure may also allow using the DIC measurements as a Non Destructive Evaluation NDE method.

If the strain field under a known load can be measured periodically, the fatigue lifetime calculations can be made as described here. Which areas are most likely to develop fiber failure can be predicted in a real component. This would also allow estimating the remaining number of cycles to failure.

4. Conclusions

Ring specimens cut from the cylindrical part of GFRP filament wound pressure vessels worked well for characterizing local fiber dominated fatigue failure around a strain concentration created by a hole. The split disk setup offers a simple alternative to pressure testing of the vessels. Changes of the strain concentrations were measured with Digital Image Correlation (DIC), allowing measurement of the entire strain field around the hole for increasing number of fatigue cycles. Production defects such as voids and thickness variation and possible undulation of fibers caused considerable local variations in the strain field that could be identified by the DIC method. However, the reasons for the changes of the strain do not need to be known. The DIC always measures the proper actual strain that causes local fatigue failure on the surface.

The maximum local static strain to failure found through DIC monitoring of static tests was found to be about two times larger than the weakest spot, a much larger variation in properties than would be expected from traditional coupon testing.

The DIC measurements showed that the strain concentrations get significantly reduced compared to the static strain field with increasing number of cycles. The reduction in strain concentrations was attributed to various forms of matrix damage developing during cycling of the specimen.

S-N curves describing local fiber damage could be found by comparing predicted Miner sum fatigue damage based on the DIC strain data and experimentally found failures. Accumulation of local fiber damage across the width of the specimen between hole and edge could be identified as the condition for catastrophic failure, i.e. the specimen breaking into two parts.

The slope of the S-N curve describing local fiber damage was the same as typical slopes for glass fiber laminates obtained from coupon specimens. However, more experimental ring test results would be needed to confirm this.

The origin of the S-N curve describing local fiber damage is significantly higher (more than a factor 2) than would be expected from standard coupon data used to characterize catastrophic failure. This means that local fatigue properties need to be properly accounted for in any characterization of the development of fatigue damage in the presence of strain concentrations.

Declaration of Competing Interest

We have no conflicts of interest to disclose.

Acknowledgements

References

[1] J.P. Berro Ramirez, D. Halm, J.-C. Grandidier, S. Villalonga, A fixed directions damage model for composite materials dedicated to hyperbaric type IV hydrogen storage vessel – Part I: Model formulation and identification, Int. J. Hydrogen Energy 40 (38) (2015) 13165–13173.

[2] T. Flatscher, H.E. Pettermann, A constitutive model for fiber-reinforced polymer plies accounting for plasticity and brittle damage including softening – Implementation for implicit FEM, Compos. Struct. 93 (9) (2011) 2241–2249.

[3] T. Ramesh, Fatigue of Composite Materials, in: H. Altenbach, W. Becker (Eds.), Modern Trends in Composite Laminates Mechanics Modern Trends in Composite Laminates Mechanics, Vienna, International Centre for Mechanical Sciences (Courses and Lectures)Springer, 2003 vol 448.

[4] ASTMASTM Standard D3039/D3039M - 17 Standard Test Method for Tensile Properties of Polymer Matrix Composite Materials, ASTM, 2017.

[5] S. Giancane, F.W. Panella, R. Nobile, R. Dattoma, Fatigue damage evolution of fiber reinforced composites with digital image correlation analysis, Procedia Eng. 2 (1) (2010) 1307–1315.

[6] W.R. Broughton, M.R.L. Gower, M.J. Lodeiro, G.D. Pilkington, M.R. Shaw, An experimental assessment of open-hole tension–tension fatigue behaviour of GFRP laminate, Compos. Part A: Appl. Sci. Manuf. 42 (10) (2011) 1310–1320.

[7] R. Talreja, W. Watt, Fatigue of composite materials: damage mechanisms and fatigue-life diagrams, Proc. R. Soc. A 378 (1981) 461–475.

[8] DNV GL, DNVGL-ST-C501 Composite Components, DNV GL, Høvik, 2017.

[9] H. Wang, W. Zhang, F. Sun, W. Zhang, A comparison study of machine learning based algorithms for fatigue crack growth calculation, Materials 10 (5) (2017).

[10] J.A. Rodriguez, Y. El-Hamzaoui, J.A. Hernandez, J.C. Garcia, J.E. Flores, A.L. Tejeda, The use of artificial neural network (ANN) for modeling the useful life of the failure assessment in blades of steam turbines, Eng. Fail. Anal. 35 (2013) 562–575.

[11] J. Mohanty, B. Verma, D. Parhi, P. Ray, Application of artificial neural network for predicting fatigue crack propagation life of aluminum alloys, Arch. Comput. Mater. Sci. Surf. Eng. 1 (3) (2009) 133–138.

[12] P. Giovanni, Numerical and Experimental Investigation of Impact Behaviour of GFRP Composiites, NTNU - Norwegian University of Science and Technology, Trondheim, 2014 (PhD thesis).

[13] M.A. Sutton, J.H. Yan, V. Tiwari, H.W. Schreier, J.J. Orteu, The effect of out-of-plane motion on 2D and 3D digital image correlation measurements, Opt. Lasers Eng. 46 (10) (2008) 746–757.

[14] S.H. Yoon, W.M. Cho, C.G. Kim, Measuremet of modulus in filament wound ring specimen using split disk test, Exp. Techn. 21 (1) (1997) 25–28.

[15] Binani and 3B, HiPertex W2020 datasheet, Binani and 3B (2015).

[16] Momentive, Technical Datasheet Epikote Resin MGS RIMR 135 and Epikure Curing Agent MGS RIMH 134 - RIMH, 2006 137, Momentive.

[17] A.E. Kraukalis, A.I. Gagani, A.T. Echtermeyer, Hygrothermal aging of amine epoxy: reversible static and fatigue properties, Open Eng. 8 (2018) 447–454.

[18] J.F. Mandell, D.D. Huang, F.J. McGarry, Fatigue of glass and carbon fiber reinforced engineering thermoplastics, Polymer Compos. 2 (3) (1981) 137–144.

[19] J.F. Mandell, D.D. Samborsky, DOE/MSU Composite Material Fatigue Database: Test Methods, Materials and Analysis, Montana State University, Montana, 1998.

[20] T.P. Philippidis, V.A. Passipoularidis, Residual strength after fatigue in composites: Theory vs. experiment, Int. J. Fatigue 29 (12) (2007) 2104–2116.

[21] Z. Hashin, Cumulative damage theory for composite materials: Residual life and residual strength methods, Compos. Sci. Technol. 23 (1) (1985) 1–19.

[22] A.T. Travesa, Simulation of Delamination in Composites Under Quasi-Static and Fatigue Loading Using Cohesive Zone Models, University of Girona, Girona, 2006.

[23] Z. Zhang, G. Hartwig, Relation of damping and fatigue damage of unidirectional fibre composites, Int. J. Fatigue 24 (2002) 713–718.

[24] P.T. Curtis, Tensile fatigue mechanisms in unidirectional polymer matrix composite materials, Int. J. Fatigue 13 (5) (1991) 377–382.

[25] V.M. Harik, J.R. Klinger, T.A. Bogetti, Low-cycle fatigue of unidirectional composites, Int. J. Fatigue 24 (2002) 455–462.

[26] L.J. Broutman, S. Sahu, A new theory to predict cumulative fatigue damage in fiberglass reinforced plastics, Compos. Mater. Test. Des. (Second Conference) (1972) 170–188 vol. ASTM STP 497.

[27] M.J. Owen, P.T. Bishop, Fatigue properties of glass-reinforced plastics containing a stress concentrator, J. Phys. D: Appl. Phys. 6 (1973) 2057–2069.

[28] E.N. Eliopoulos, T.P. Philippidis, A progressive damage simulation algorithm for GFRP composites under cyclic loading. Part I: Material constitutive model, Compos. Sci. Technol. 71 (5) (2011) 742–749.

[29] Z. Fawaz, F. Ellyin, Fatigue failure model for fibre-reinforced materials under general loading conditions, J. Compos. Mater. 28 (15) (1994) 1432–1451.